AUV Geophysical Navigation using Magnetic Data - the MEDUSA GN system

João Quintas
Institute for Systems and Robotics,
Instituto Superior Técnico,
Univ. Lisboa,
Av. Rovisco Pais 1, 1049-001
Lisbon, Portugal

Francisco Curado Teixeira
Institute of Electronics and
Informatics Engineering of Aveiro,
University of Aveiro,
Campus Univ. de Santiago, 3810-193
Aveiro, Portugal

António Pascoal
Institute for Systems and Robotics,
Instituto Superior Técnico,
Univ. Lisboa,
Av. Rovisco Pais 1, 1049-001
Lisbon, Portugal

***Abstract*—This paper reports recent advances on the development of geophysical navigation (GN) algorithms for small, affordable autonomous underwater vehicles. The successful results obtained by the authors during prior work on magnetic-based GN algorithms (MAGNAV), tested in computer simulations, motivated the implementation of a GN module to be incorporated in the Robotic Operating System (ROS) installed on an autonomous marine vehicle of the MEDUSA class. The development effort included: acquisition of prior magnetic maps in an offshore area of Lisbon; execution of data-acquisition tests using a MEDUSA vehicle equipped with a towed magnetometer; development of the *medusa_gn* package and its test as GN module of the ROS system installed in the MEDUSA. A realistic assessment of the performance of the MAGNAV method was performed in simulations by exploiting, for the first time, the ROS capability of playing back the recorded data as if the vehicle were operating in real-time. The results obtained in the present work confirm the good performance of the MAGNAV filter observed in former tests in terms of position estimation and motivate a new series of tests aiming at the validation of GN algorithms in real-time navigation experiments.**

***Index Terms*—autonomous underwater vehicle, geophysical navigation, magnetic navigation, particle filter**

I. Introduction

True autonomous navigation of underwater robotic vehicles is still a challenging problem due mainly to the operational difficulties posed by the underwater environment. Without access to the Global Position System (GPS) and in the absence of acoustic beacons whose deployment is costly and complex, the navigation of autonomous underwater vehicles (AUV) is normally performed by dead-reckoning (DR). Conventional DR based on the integration of data from an attitude and heading reference system (AHRS) and a Doppler velocity logger (DVL) is a convenient technique for relatively short-range and time-limited navigation but, as is well-known, the position error resulting from this solution will grow over time, making it difficult to achieve precise navigation when dead-reckoning is used for a long period of time. Over the past few years, geophysical navigation (GN) has been proposed as the method of choice to aid AHRS/DVL navigation of underwater vehicles, due the relatively low-cost of GN implementations and its potential to provide accurate estimates of position in the short term combined with bounded localization errors in the long run. In order to estimate the position of robotic vehicles, GN methods exploit geophysical effects observed in the environment, such as terrain topography, gravity, and the geomagnetic field. A conventional implementation of underwater geophysical navigation is the well-studied terrain-aided navigation (TAN) method which relies exclusively on matching a set of range measurements acquired with sonar sensors installed on a vehicle with a previously acquired digital elevation map (DEM) of the terrain to estimate position. The work of Nygren and Jansson [1], Anonsen and Hallingstad [2], and Morice et al. [3], among others, demonstrated experimentally the potential of the TAN solution in different types of terrain and with distinct sensor suites. Despite these successful implementations, the performance of terrain-based navigation systems depends strongly on the availability of topographic information. It is well known that large areas of the ocean floor are characterized by a very smooth, mostly flat topography where GN implementations become ineffective due to the the lack of exciting terrain features. To implement geophysical navigation solutions in this type of environments it is necessary to exploit other types of information, such as that available from the Earth's gravitic and magnetic fields, which may lead to alternative GN solutions capable of yielding better positioning accuracy. The rationale for this approach arises from the fact that important anomalies from other geophysical effects are often found in areas of the seafloor characterized by insufficiently excited terrain topography. The interested reader may find a recent, comprehensive survey of the sate of the art on TAN and GN in the work of Teixeira et al. [4] and Melo and Matos [5].

A. Problem motivation

From the alternative GN methods proposed in the literature, geomagnetic navigation (MAGNAV) appears as one of the most interesting due to its relatively low cost and potential in terms of acquistion of terrain information. Instead of relying on global or regional models of the geomagnetic field, the MAGNAV approach exploits the ubiquitous, local magnetic disturbances of the main-field caused by geological bodies or man-made artifacts that manifest themselves in the form of small-intensity anomalies of short wave-length. The method

resides essentially in matching measurements of the total magnetic field intensity observed locally by a surveying vehicle with a prior map of the terrain.

The potential of magnetic-based geophysical navigation to estimate the position of a marine vehicle has been confirmed, mainly in computer simulations with synthetic and real data, in the works of Tyren [6], Teixeira and Pascoal [7], Kato and Shigetomi [8], Quintas et al. [9], and Guo et al. [10], adopting different types of magnetic sensors and estimation methods. More recently the work of Teixeira et al. [11] describes an experimental proof of the concept using a marine robotic vehicle.

This paper describes the work done towards the implementation of a magnetic-based geophysical navigation module that can be integrated with the dead-reckoning navigation systems of the Medusa-class of hybrid AUV/ASV, developed and operated by the Institute for Systems of Robotics of Instituto Superior Tcnico (ISR-IST), Lisbon, Portugal. Relying on prior work by the authors [12], the paper proposes a Rao-Blackwellized particle filter (RBPF) as the core navigation algorithm. The RBPF mechanizes a data fusion procedure using a marginalized particle filter which estimates the 2D position of the vehicle as well as the 2D components of the velocity bias incurred by dead-reckoning. The RBPF is implemented as a single ROS node in the vehicle's software architecture that combines a vehicle motion model fed by data from an AHRS and a DVL and a measurement model associated with a total field magnetometer. All sensor and control messages were recorded in a ROS bagfile, thus ensuring that all messages were associated with their corresponding time-stamps. Based on the information acquired, and using standard ROS tools, the data can be played back and the Medusa navigation experiments can be simulated with the real data as if the vehicle were operating in real-time.

II. Basic Notation, Problem Formulation, and Navigation Filter Setup

A. Problem formulation and notation

In what follows, we borrow the notation and the corresponding design models from [13], where the reader can find additional details of the formulation of the current navigation problem. The following notation will be used:

- $\{I\}$: inertial coordinate frame;
- $\{B\}$: body-fixed frame that moves with the vehicle;
- $\mathbf{p} = [x, y, z]^T$: position of the origin of $\{B\}$ measured in $\{I\}$;
- $\lambda = [\phi, \theta, \psi]^T$: roll, pitch and yaw that parametrize locally the orientation of $\{B\}$ relative to $\{I\}$;
- $\omega = [p, q, r]^T$: angular velocity of $\{B\}$ w.r.t. $\{I\}$, expressed in $\{B\}$;
- $V = [u, v, w]^T$: linear velocity of the origin of $\{B\}$ relative to the sea-bottom, expressed in $\{B\}$.

The MAGNAV problem discussed here is considered a non-linear estimation problem due to the nonlinear, non-structured nature of the measurement model which relates measurements provided by the magnetic sensors deployed by the vehicle with its three-dimensional position and orientation relative to the sea-bottom represented in a map. The problem is addressed here in the framework of nonlinear sequential Monte Carlo estimation, using the prior-correction particle filter (PPF) described in [13]. We adopt the notation usually associated with the formulation of particle filters; see e.g. the comprehensive list of references included in [4].

The current problem can be restricted to the estimation of position and velocity in the horizontal plane, given the following assumptions:

- The AUV maintains a constant depth (z);
- The AUV is levelled horizontally and stabilized in roll and pitch, i.e. $\phi = \theta = 0$.

The first assumption is fundamental in terms of the current implementation of the GN concept. Actually, the magnetic field readings obtained in real-time by the vehicle sould be acquired at approximately the same (constant) altitude to which the prior magnetic data is referenced in order to maximize correct map-matchings. This requirement also eliminates the need to estimate de depth, allowing z to be treated as an input instead of a state variable. The second assumption permits treating $r = \dot{\psi}$ as the angular velocity (yaw rate) of the vehicle. By postulating these assumptions, the linear velocity of the vehicle is represented by vector $\mathbf{v} = [\dot{x}, \dot{y}]^T$.

B. Stochastic models and filter set-up

The formulation of the process and measurement models is taken with minor modifications from [13] and is summarized as follows:

- $\mathbf{x}$: vector representing the system state with dimension n_x;
- $\mathbf{y}$: measurement vector with dimension n_y;
- N: number of samples (particles) used by the particle filter;
- $\mathbf{x}_t^i$: represents the i^{th} particle (a random sample from the state space) at time instant t;
- ω_t^i: weight associated to particle $\mathbf{x}_t^i$.

1) Process model: The discrete-time kinematic model that we consider is described by

$$\mathbf{x}_{k+1} = F\mathbf{x}_k + G_{u,k}\mathbf{u}_k + L\zeta_k, \tag{1}$$

where:

- $F = I_{2\text{x}2}$: state-transition matrix;
- L: noise coupling matrix;
- $\mathbf{x} = [x, y]^T$: state-vector;
- $\mathbf{u}_k = [u, v, \psi]^T$: input vector;
- $\zeta_k \in \mathbb{R}^{n_x}$: process noise sequence;
- $G_{u,k}$: input coupling matrix, function of the orientation ψ;

- $G_{u,k}\mathbf{u}_k$: dead-reckoning incremental displacement which is a function of linear velocity and orientation.

This kinematic model relies on the velocity vector supplied by a simplified version of the dynamic model embodied in the inner control loop of the MEDUSA autonomous marine vehicle. The reader interested in additional details about this topic is referred to the recent publication [14].

2) Measurement model: The discrete-time measurement model with additive measurement noise is given by

$$\mathbf{y}_k = h(\mathbf{p}_k, \psi) + \eta(\mathbf{p}_k, \psi), \tag{2}$$

where $h(.) : \mathbb{R}^4 \rightarrow \mathbb{R}^{n_y}$ is a function that yields the magnetic field measured by the vehicle at a given position, $\mathbf{p}_k$. We note that the total magnetic field readings used in this work are scalar measurements. As a consequence, the magnetic observation model is not parametrized by the orientation angle ψ. However, the expression presented in (2) is made sufficiently general to account for non scalar magnetic readings, for example, when using vector magnetometers; in this case, $h(\mathbf{p}_k, \psi)$ is a function of the vehicle orientation, denoted ψ. The set of measurements taken at each iteration is represented by vector $\mathbf{y_k}$ and $\eta \in \mathbb{R}^{n_y}$ models map errors and measurement noise. Notice that this model can be easily modified to include an additional scalar measurement such as the vehicle altitude.

3) Noise models: Given information on the vehicle position and orientation, the measurement noise variables represented in the vector η are considered mutually independent and are characterized by the measurement noise intensity matrix Rk. The discrete-time process noise sequences represented in ζ_k are assumed mutually independent and Gaussian, with intensity noise represented by matrix Q.

III. GN Navigation Filter Set-up

A. Marginalized particle filter

The good results obtained in prior work with GN methods based on Rao-Blackwellized particle filters (RBPF) justify the adoption of this class of estimators in the present work. The structure of the navigation filter adopted here is similar to the one defined in [13]. Using this formulation, the state vector is decomposed into two parts: $\mathbf{x} = [\mathbf{x^{pf}}, \mathbf{x^{kf}}]^\mathbf{T}$, where $\mathbf{x}^{pf} = [x, y]^T$ represents the part of the state vector estimated by the PF and $\mathbf{x}^{kf} = [b_x, b_y]^T$ is the part of the state vector estimated by a Kalman Filter (KF). A corresponding decomposition is adopted for the state transition matrix F, the input coupling matrix $G_{u,k}$, the noise coupling matrix L, the input and noise vectors $\mathbf{u}_k$ and ζ_k, and the discrete-time process noise intensity matrix Q; the input vector is defined as $\mathbf{u}_k = [u_k, v_k, \psi_k]^T = [V_k, \psi_k]^T$. According to this convention, the RBPF formulation becomes:

Prediction

$$\mathbf{x}_{k+1}^{pf,i} = \mathbf{x}_k^{pf,i} + F^{pf}\mathbf{x}_k^{kf,i} + G_{u,k}^{pf}V_k + \zeta_k^{pf} \tag{3}$$

$$\mathbf{x}_{k+1}^{kf,i} = F^{kf}\left[\hat{\mathbf{x}}_{k|k-1}^{kf,i} + K_k\nu_k\right] \tag{4}$$

where K_k denotes the KF gain,

$$\nu_k = \mathbf{x}_{k+1}^{pf,i} - \mathbf{x}_k^{pf,i} - \left(F^{pf}\hat{\mathbf{x}}_{k|k-1}^{kf,i} + G_{u,k}^{pf}V_k\right), \text{ and}$$

$$\zeta_k^{pf} \sim \mathcal{N}\left(0, F^{pf}P_{k|k-1}^{kf}\left(F^{pf}\right)^T + L^{pf}Q^{pf}\left(L^{pf}\right)^T\right). \tag{5}$$

Update

The update of the weights is performed according to the expression:

$$w_k^i = w_{k-1}^i p(\mathbf{x}_k|\mathbf{x}_{k-1}^i)p(\mathbf{y}_k|\mathbf{x}_k^i). \tag{6}$$

This version of the PF is designated prior-correction particle filter (PPF) [13]. The filtering step of the PPF is applied to the joint likelihood of the measurements and the current state conditioned on the prior state, instead of using only the measurement likelihood like a standard PF. The advantages and disadvantages of applying a PPF are analysed in depth in [4].

Point estimates

At any given iteration k of the filter, a point estimate of the current state $\hat{\mathbf{x}}_k$ and the associated covariance matrices P_k can be obtained from the following equations:

$$\hat{\mathbf{x}}_k^{MMS} \simeq \sum_i^N \omega_k^i \mathbf{x}_k^i = \sum_i^N \omega_k^i \begin{bmatrix} \mathbf{x}_k^{pf,i} \\ \mathbf{x}_k^{kf,i} \end{bmatrix} \tag{7}$$

$$P_k^{pf} = \sum_i^N \omega_k^i \left(\mathbf{x}_k^{pf,i} - \hat{\mathbf{x}}_k^{pf,MMS}\right) \cdot \left(\mathbf{x}_k^{pf,i} - \hat{\mathbf{x}}_k^{pf,MMS}\right)^T \tag{8}$$

$$P_k^{kf} = P_{k|k}^{kf} + \sum_i^N \omega_k^i \left(\hat{\mathbf{x}}_{k|k}^{kf,i} - \hat{\mathbf{x}}_k^{kf,MMS}\right)\left(\hat{\mathbf{x}}_{k|k}^{kf,i} - \hat{\mathbf{x}}_k^{kf,MMS}\right)^T. \tag{9}$$

IV. In-water data collection

The magnetic data used in the present work were acquired at sea in two phases. In the first phase, a new area of tests was surveyed to acquire the prior total field intensity map required by the MAGNAV method. The second phase consisted of a series of three experiments with the MEDUSA vehicle towing a total field magnetometer. The geophysical information and the navigation data collected with the MEDUSA vehicle was later used to validate the MAGNAV method in simulations. The following sections report on the rationale of the experimental tests, the equipment used in the trials, and the data-acquisition work.

A. Prior map

1) Selection of a new trial site: The data used in prior work by the authors was collected in a shallow-water lake with an area of approximately $300m$ x $200m$ located at *Doca do Oceanrio - Parque das Nações*, in Lisbon. This site is frequently used by the ISR/IST team in its marine robotics experiments due mainly to the accessibility of the area and the simplicity of the associated logistics. As reported in previous works, the site proved to be valuable to validate the application of magnetic based GN algorithms in experimental tests, despite the scarcity of magnetic anomalies observed in the area, the reduced area available for maneuvering, and the shallow water environment. However, in order to assess the performance of the proposed GN solution in a wider diversity of realistic operational conditions, it was decided to perform the new tests at sea, in the offshore of Lisbon.

The new site chosen for tests is located offshore *S. Pedro do Estoril*, near Lisbon; see map in Fig. 1. The choice was dictaded primarily by the availability of significant magnetic information associated to a series of magnetic anomalies observed in the area, as documented in geophysical maps provided by the Instituto Português do Mar e da Atmosfera (IPMA). It is worth noting that this area is located in open-sea and subjected to strong oceanic currents which are normally detrimental for navigation solutions based on dead-reckoning and also represents an increased challenge for geophysical-based navigation.

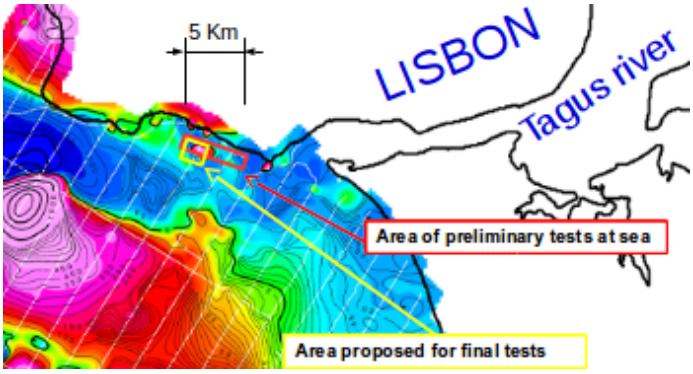

Fig. 1. Geographic region, and geo-magnetism of the test area. Notice the significant magnetic anomalies observed in the area where the final tests have been conducted.

B. Acquisition and processing the data of the prior map

A preliminary survey with very-high spatial resolution, consisting of closely spaced transects executed with the marine magnetometer towed by a small boat, was performed in the first phase of this work in order to obtain a precise a priori magnetic maps of selected zones of the test area; see the lines in red in Fig. 2. The final site for tests with an area of approximately $600m$ x $600m$ was then selected based on the analysis of the previously acquired data; see the blue squared region in Fig. 2.

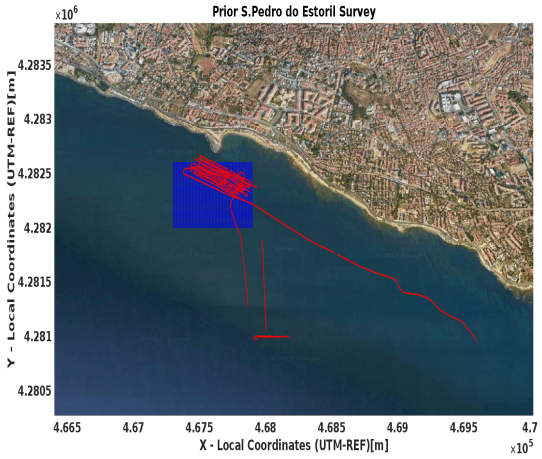

Fig. 2. Aerial view and geographic location of the offshore region, transects of data acquisition executed during the exploratory survey (red lines), and shaded blue grid corresponding to the area selected for the final tests based on the prior magnetic maps and the magnetic data acquired in the exploratory survey.

The test area was surveyed with a magnetic gradiometer comprising two *Marine Magnetics Explorer* total field magnetometers. The *Marine Magnetics Explorer* sensor encapsulates a total field Overhauser magnetometer with an absolute accuracy of 0.2nT, a sampling frequency range of 0.1Hz to 4Hz, a power comsuption of 2W, and an operating range from 18000nT to 120000nT.

The structure that holds the two magnemoters is made of non ferromagnetic material to avoid corrupting the magnetic readings. The sensor arrangement employed constitutes a magnetic gradiometer equipped with a GPS antenna on top, which permits an accurate localization of the data acquired with the towed system; see the schematic depicted in Fig. 3.

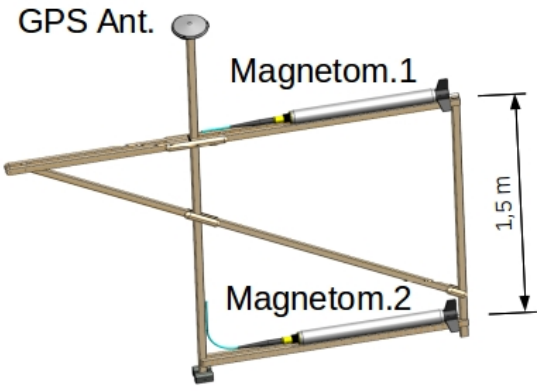

Fig. 3. Schematic magnetic gradiometer assembly.the magnetic data acquired in the exploratory survey.

The gradiometer was towed $10m$ behind the boat in order to mitigate the magnetic disturbances from the vessel structure. The results of this survey were a set of three distinct maps,

including two total field intensity maps acquired at distinct altitudes (sea surface and $1.5m$ depth) and a differential magnetic field map of the same area. The prior map used to validate the MAGNAV method is shown in Figs. 4 and 6 and corresponds to the data acquired with the magnetometer at the sea surface. The map has the dimension of $600m$ x $530m$ and a $1m$ grid resolution.

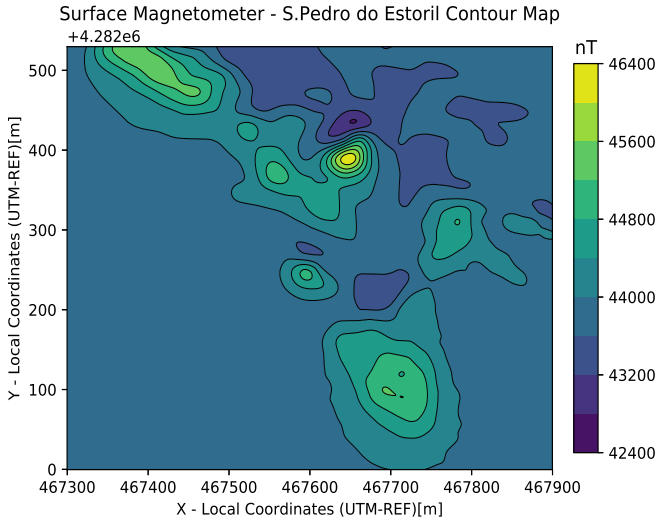

Fig. 4. Map of total magnetic field intensity observed at the sea surface in the test area.

The map show the high variability of magnetic features present at the site. It it is important to notice however, the existence of a large area devoid of observable magnetic features in the Western part. The final survey lines used to produce the map are represented in Fig. 5. Although the planned spacing of the survey lines was $5m$, due to adverse weather conditions and time limitations, it was not possible to execute all the transects as planned; several lines had to be done with double spacing, $10m$.

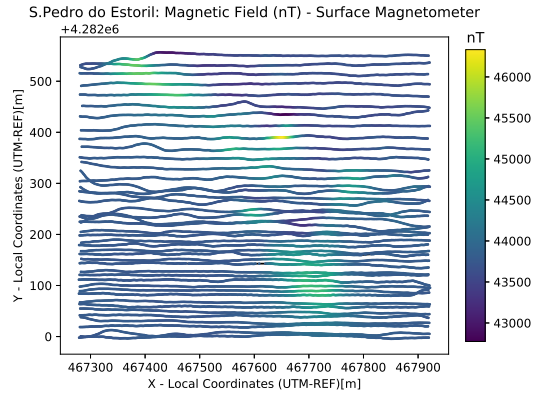

Fig. 5. Survey lines used for processing the prior total intensity field magnetic map, with color scale representative of measured magnetic field intensity).

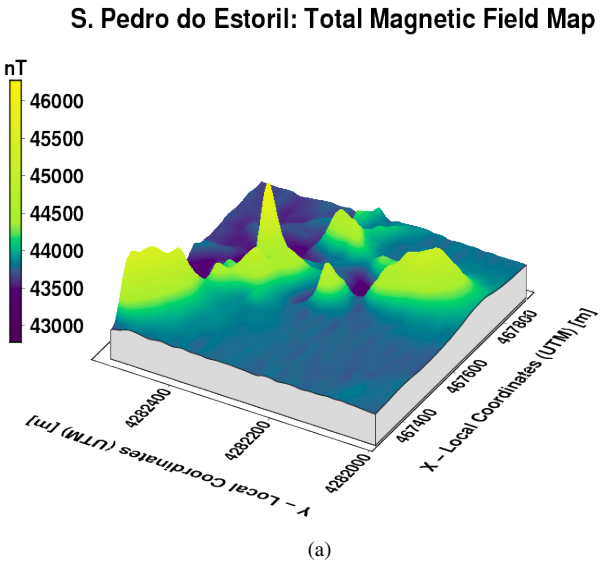

(a)

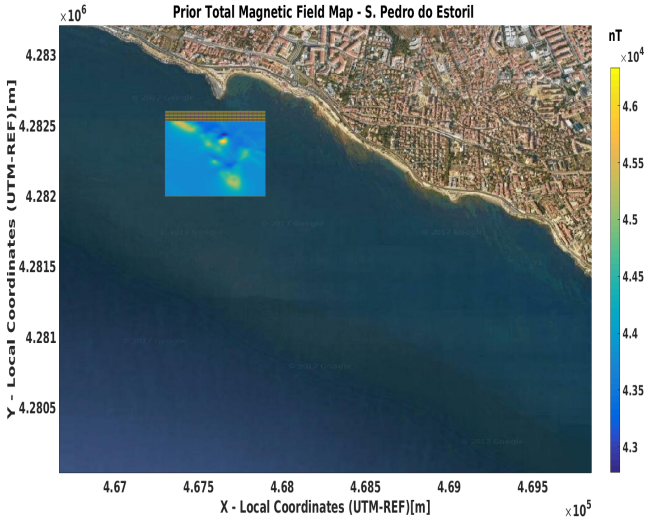

(b)

Fig. 6. (a) - Total magnetic field map of S. Pedro do Estoril; (b) - Total magnetic field map superimposed on a satellite map of S. Pedro do Estoril area.

C. Magnetic data acquisition with the MEDUSA vehicle

1) The MEDUSA class vehicle: The robotic platform used in this work is the autonomous vehicle of the MEDUSA class designed, built, and operated by the Institute for Systems and Robotics of IST, Univ. de Lisboa, Portugal [14]; see a schematic illustration of the vehicle in Fig. 7 and its main characteristics in Table. I. The MEDUSA is a double-body robotic marine vehicle that can be configured as an autonomous surface vehicle (ASV) or an autonomous underwater vehicle (AUV).

Since the main objective of this work was to evaluate the performance of the MAGNAV method, the MEDUSA was operated in the ASV configuration, which incorporates a GPS-RTK used to localize the vehicle precisely. These data were

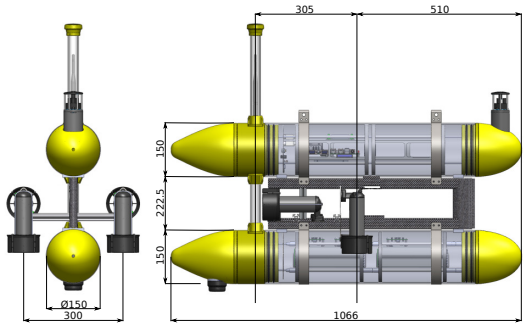

Fig. 7. A schematic illustration of the MEDUSA side and back views with dimensions in millimeters.

TABLE I
MAIN CHARACTERISTICS OF THE MEDUSA CLASS VEHICLE

Vehicle Type	ASV, AUV
Communications	Wireless (surface) + acoustic modem (u.w.)
External positioning	GPS-RTK (ASV) + USBL (AUV)
Height	875 mm
Width	350 mm
Length	1066 mm
Body diameter	150 mm
Weight in the air	from 270 Kg
Energy	830 Wh LIPO battery cluster
Endurance	11 hrs at 1,5 knots
Propulsion system	Diver version: 4 thrusters

used as ground truth to assess the performance of the proposed navigation filter.

Some details of the magnetometer installation in the MEDUSA can be observed in Fig. 8. The magnetometer is towed with a layback of $5m$ in order to mitigate the effects of the electromagnetic noise introduced by the vehicle in the magnetic readings. The main disadvantage of this sensor arrangement is the lateral deviation that can be imparted to the towed magnetometer relativelly to the trajectory followed by the vehicle, by oceanic currents and wind (when deployed at the sea-surface). These unobservable drifts may impact negativelly the performance evaluation of GN methods because the online magnetic readings will not match the values mapped a priori which are retrieved from prior maps based on the position obtained from the ASV-mounted GPS. This problem is especially notorious when the vehicle navigates in areas characterized by strong magnetic gradients. In this type of scenario, even a small error in the estimated position of the magnetic sensor introduces large discrepancies between the real-time readings and the mapped values that may lead to poor performance of the navigation filters used for precise, short-range navigation (as in the present case).

The integration of the package responsible for the magnetic data acquisition and the geophysical navigation module with the remaining software of the MEDUSA exploited the versatility of the software architecture, which is supported by the ROS system running on the MEDUSA vehicles, see Fig. 9.

Fig. 8. Magnetic sensor cabling and connection to the Medusa ASV.

In the present work, a new ROS node was developed to work as a driver of the magnetometer, being responsible for the acquisition of the magnetic readings.

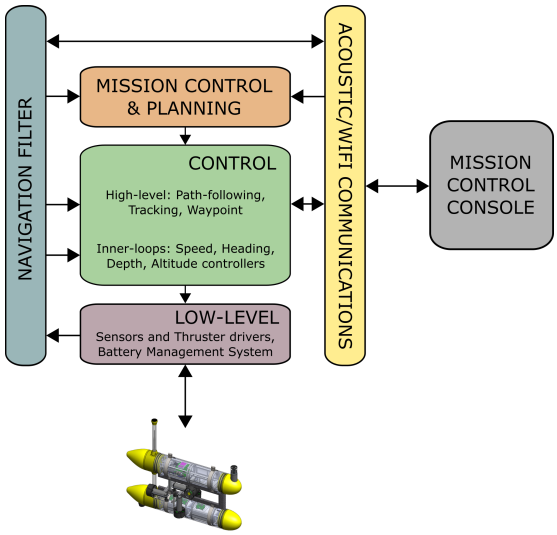

Fig. 9. Simplified diagram of the software architecture on the MEDUSAs.

2) GN sea trials with the MEDUSA: During the sea trials, the operation of the Medusa ASV was supervised by a support vessel maneuvering in its proximity and connected to the vehicle via a wireless communication link. This close supervision allowed for real-time monitoring of the vehicle's state and the quality of terrain-related data-acquisition. The MEDUSA moved with a surge velocity of $0.5m/s$ and the magnetic readings were acquired at $1Hz$, corresponding to a distance between sampling points along the transects of approximately $0.5m$. All sensor and control messages were recorded in a ROS bagfile.

The tests consisted of three experiments with the following main characteristics:

1) Mission one - the first trial corresponding to a rectangular trajectory of $200m$ x $150m$; 2) Mission two - a second one in the form of a square path with $300m$ x $300m$; 3) Mission three

- a lawn-mowing maneuver covering an area of approximately $200m$ x $150m$.

V. Presentation and Discussion of Experimental Results

This section details the results obtained with the MAGNAV method fully integrated with the MEDUSA's software arquitecture, based on a new ROS node which was developed for this purpose and integrated in the control module of the MEDUSA vehicle. Besides estimating the position of the vehicle, this node is also responsible for syncronizing the data received from the magnetometer with other sensors messages.

A. *Mission one* - $200m$ *x* $150m$ *rectangle*

Start Pos: $X = 310\ Y = 400$ | *End Pos:* $X = 366\ Y = 400$

The accuracy of position estimaton achieved by the filter in the first two legs of this mission is worse than expected based on our prior experience in confined waters. The observed degradation of positioning accuracy is explained by the error introduced by the method of ground-truthing that relies on the GPS position acquired by the vehicle, from which the position of the magnetomer is deduced by subtraction of the layback. This approach is valid only when the towed sensor follows the same path of the vehicle with minimum lateral drift, a condition that was frequently violated in the tests, due to unobservable currents and wind ocurring in the open sea. This effect can observed in the first two legs (WE and NS directions) shown in Fig.11. From the middle of the third leg the filter recovers and the magnitude of the position error decreases. Until the end of the test, the magnitude of the position error achieved with the MAGNAV method remains lower than the one obtained by dead-reckoning; see Fig 10. The final position estimated by the MAGNAV method is significantly more accurate than that obtained by dead-reckoning.

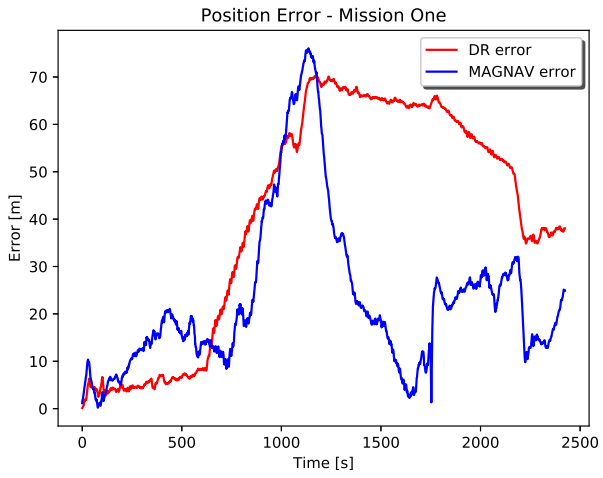

Fig. 10. Mission one - Comparison of the position estimation errors achieved by dead-reckoning and the MAGNV filter.

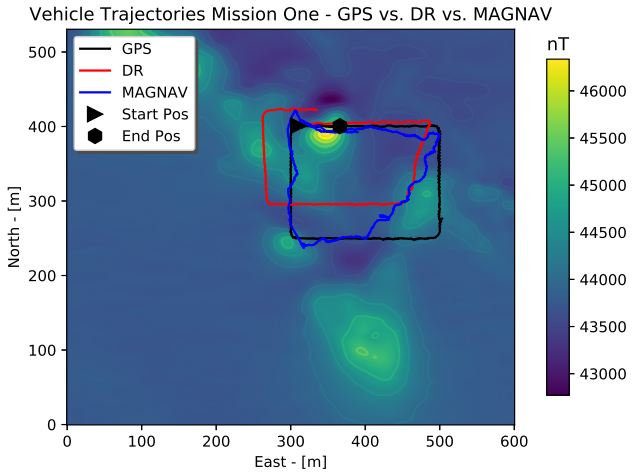

Fig. 11. Mission one - Real trajectory followed by the vehicle, compared with the trajectory estimated by dead-reckoning and the MAGNAV filter.

B. *Mission two* - $300m$ *x* $300m$ *square*

Start Pos: $X = 536\ Y = 100$ | *End Pos:* $X = 330\ Y = 100$

In general, the magnitude of the estimation error achieved in this mission with the MAGNAV filter is smaller than the one obtained by dead-reckoning, as can be seen in Fig. 12. The largest error incurred by MAGNAV occurs in the area without magnetic information shown in Fig. 13.

Fig. 12. Mission two - Comparison of the position estimation errors achieved by dead-reckoning and the MAGNV filter.

C. *Mission three - lawn-mowing*

Start Pos: $X = 134\ Y = 228$ | *End Pos:* $X = 346\ Y = 349$

The magnitude of the position error obtained by MAGNAV is below $10m$, in general, as can be seen in Fig.14. The error increases in the first part of the mission where there are no magnetic features - see Fig.15 - and in a small part just

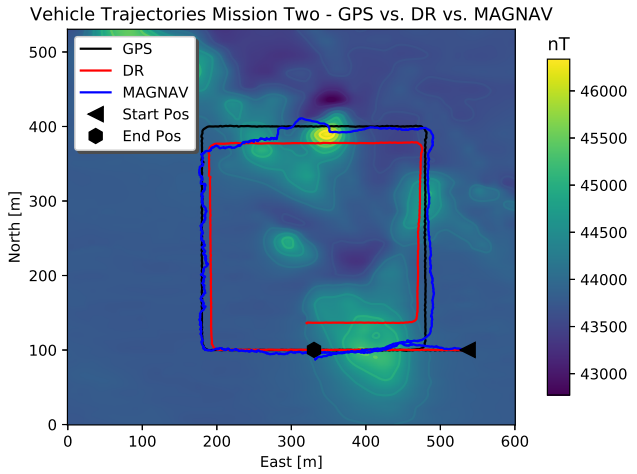

Fig. 13. Mission two - Real trajectory followed by the vehicle, compared with the trajectory estimated by dead-recknoning and the MAGNAV filter.

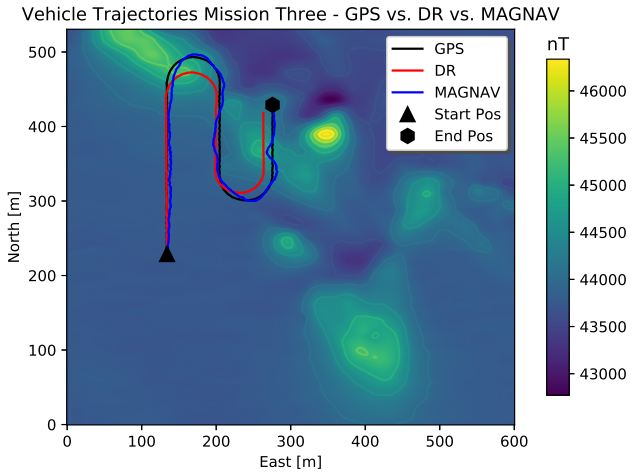

Fig. 15. Mission three - Real trajectory followed by the vehicle, compared with the trajectory estimated by dead-recknoning and the MAGNAV filter.

before the second curve, where the position estimation error of MAGNAV is larger than the dead-reckoning error. The larger error observed in this area is associated with a lateral drift of the magnetometer relativelly to the trajectory of the vehicle, a problem that cannot be solved with the current configuration of the ground-truth system, as explained above. Despite the somewhat reduced accuracy achieved by MAGNAV in this mission, it is worth noting that the errors of GN estimates of position remain bounded whereas the dead-reckoning error is not bounded and tends to grow with time and distance travelled.

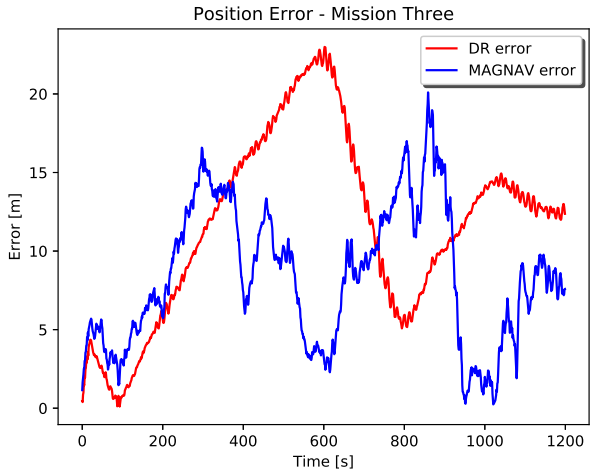

Fig. 14. Mission three - Comparison of the position estimation errors achieved by dead-reckoning and the MAGNV filter.

VI. Conclusions

The main purpose of the work described was to assess the performance of magnetic-based navigation algorithms integrated for the first time in the ROS-based software architecture of the MEDUSA AUV/ASV. For this purpose, a set of prior magnetic maps were collected in a preliminary phase and a series of experimental trials were performed later with the ASV instrumented with a towed total-field magnetometer. The hardware and software configurations were designed to mimic the real set-up that will be used in future tests of geophysical navigation in real-time.

The sea-trials were conducted in the open sea, where the vehicle-magnetometer system was exposed to very realistic and challenging operational conditions. In this scenario, the performance of the GN filters was affected by significant drifts imparted to the towed magnetometer by oceanic currents and wind. Despite these detrimental effects, the results so obtained confirm the high potential of the MAGNAV filter to achieve bounded positioning estimation errors. The encouraging results obtained in these experiments motivate the execution of real-time navigation experiments with the Medusa AUV, which will be conducted in the very near future.

Acknowledgment

The authors are indebted to the colleagues at ISR/IST who gave technical support to the missions at sea and provided valuable advice to carry out the experimental tests. We are also indebted to the team Estrutura de Missão para a Extensão da Plataforma Continental - EMEPC who kindly provided the vessel for the surveys. A special word of thanks goes to the EMEPC team members António Calado, Andreia Afonso, and Bruno Ramos for the willingness to aid us in the surveys. Finally, we are grateful to Dra. Marta Neres and Dr. Pedro

Terrinha from IPMA for helping us select the test site described in this work.

REFERENCES

[1] I. Nygren and M. Jansson, "Terrain navigation for underwater vehicles using the correlator method," *IEEE Journal of Oceanic Engineering*, vol. 29, no. 3, pp. 906–915, July 2004.

[2] K. B. Anonsen and O. Hallingstad, "Terrain aided underwater navigation using point mass and particle filters," in *2006 IEEE/ION Position, Location, And Navigation Symposium*, April 2006, pp. 1027–1035.

[3] C. Morice, S. Veres, and S. McPhail, "Terrain referencing for autonomous navigation of underwater vehicles," in *OCEANS 2009-EUROPE*, May 2009, pp. 1–7.

[4] F. C. Teixeira, J. Quintas, P. Maurya, and A. Pascoal, "Robust particle filter formulations with application to terrain-aided navigation," *International Journal of Adaptive Control and Signal Processing*, vol. 31, no. 4, pp. 608–651, 2017, acs.2692. [Online]. Available: http://dx.doi.org/10.1002/acs.2692

[5] J. Melo and A. Matos, "Survey on advances on terrain based navigation for autonomous underwater vehicles," *Ocean Engineering*, vol. 139, pp. 250–264, 2017. [Online]. Available: http://www.sciencedirect.com/science/article/pii/S002980181730241X

[6] C. Tyren, "Magnetic terrain navigation," in *Unmanned Untethered Submersible Technology, Proceedings of the 1987 5th International Symposium on*, vol. 5, Jun 1987, pp. 245–256.

[7] F. C. Teixeira and A. M. Pascoal, "7th IFAC Conference on Control Applications in Marine Systems GEOPHYSICAL NAVIGATION OF AUTONOMOUS UNDERWATER VEHICLES," *IFAC Proceedings Volumes*, vol. 40, no. 17, pp. 117–122, 2007. [Online]. Available: http://www.sciencedirect.com/science/article/pii/S1474667015320814

[8] N. Kato and T. Shigetomi, "Underwater Navigation for Long-Range Autonomous Underwater Vehicles Using Geomagnetic and Bathymetric Information," *Advanced Robotics*, vol. 23, no. 7-8, pp. 787–803, 2009. [Online]. Available: http://dx.doi.org/10.1163/156855309X443016

[9] J. Quintas, F. C. Teixeira, and A. Pascoal, "Magnetic signal processing methods with application to geophysical navigation of marine robotic vehicles," in *OCEANS 2016 MTS/IEEE Monterey*, Sept 2016, pp. 1–8.

[10] C. Guo, H. Cai, and G. van der Heijden, "Feature Extraction and Geomagnetic Matching," *Journal of Navigation*, vol. 66, pp. 799–811, 11 2013.

[11] F. C. Teixeira, J. Quintas, and A. Pascoal, "Experimental validation of magnetic navigation of marine robotic vehicles**funding: This research was supported in part by the european project wimust (ga no. 645141) and the portuguese fct funding program [pest-oe/eei/la0009/2011]. the authors gratefully acknowledge the sponsorhip of the south korean agency for defense development under a collaborative research agreement between kaist and ist." *IFAC-PapersOnLine*, vol. 49, no. 23, pp. 273–278, 2016, 10th IFAC Conference on Control Applications in Marine SystemsCAMS 2016. [Online]. Available: http://www.sciencedirect.com/science/article/pii/S2405896316319413

[12] F. Curado, J. Quintas, and A. Pascoal, "4th IFAC Workshop onNavigation, Guidance and Controlof Underwater VehiclesNGCUV 2015 AUV Terrain-Aided Navigation using a Doppler Velocity Logger," *IFAC-PapersOnLine*, vol. 48, no. 2, pp. 137–142, 2015. [Online]. Available: http://www.sciencedirect.com/science/article/pii/S240589631500261X

[13] F. C. Teixeira, A. Pascoal, and P. Maurya, "3rd IFAC Workshop on Navigation, Guidance and Control of Underwater Vehicles A Novel Particle Filter Formulation with Application to Terrain-Aided Navigation," *IFAC Proceedings Volumes*, vol. 45, no. 5, pp. 132–139, 2012. [Online]. Available: http://www.sciencedirect.com/science/article/pii/S1474667016305924

[14] P. C. Abreu, J. Botelho, P. Góis, A. Pascoal, J. Ribeiro, M. Ribeiro, M. Rufino, L. Sebastião, and H. Silva, "The MEDUSA class of autonomous marine vehicles and their role in EU projects," in *OCEANS 2016 - Shanghai*, April 2016, pp. 1–10.